Vacuum 165 (2019) 232–238

Contents lists available at ScienceDirect

Vacuum

journal homepage: www.elsevier.com/locate/vacuum

Uncertainty evaluation and phase variation of ultrasonic interferometer manometer: A primary pressure and vacuum standard

Ashok Kumar[a,b,*], Vikas N. Thakur[a,b], Rakesh Sharma[a], Harish Kumar[a], Omprakash[a], Sanjay Yadav[a,b]

[a] CSIR-National Physical Laboratory (CSIR-NPL), Dr. K. S. Krishnan Road, Delhi, 110012, India
[b] Academy of Scientific and Innovative Research (AcSIR), CSIR- NPL Campus, Dr. K. S. Krishnan Road, Delhi, 110012, India

ARTICLE INFO

Keywords:
UIM
Primary pressure standard
Uncertainty
Measurement
Phase angle

ABSTRACT

The ultrasonic interferometer manometer (UIM) is an apex level primary pressure standard for Pascal realization established at National Physical Laboratory India (NPLI). The performance of UIM has been evaluated from time to time by participation in key comparisons, calibration and measurement capabilities (CMC) and publications in reputed international metrology journals. The pressure is measured using time of flight technique at 44 different frequencies in ultrasonic range and the phase measurement. The phase measurement combined with the time of flight measurement using the exact fractional algorithm provides highly accurate column length hence respective pressure values. The combined process helps in lowering the uncertainty in real experimental conditions. Recently, we have also changed UIM software from tbasic to window based program with the same algorithm which provides a column length measurement study. A detailed study was carried out for variation of fringe counts or oscillations with varying pressure. Experimental and theoretical calculation for both resolution and pressure dependent part has been carried out for uncertainties involves the physical parameters. The uncertainties in lower pressure range, i.e., between 1 Pa and 1000 Pa were varying equal or sometimes higher than the theoretical resolution value 0.0092 Pa ($k = 2$) because of environmental conditions like vibration, temperature, atmospheric pressure, and humidity whereas for higher pressure range, i.e., 1000 Pa to 130 kPa the uncertainties were either close or smaller than the pressure dependent theoretical uncertainty value, i.e. 7.2×10^{-6} of the reading.

1. Introduction

The UIM, an apex level primary pressure standard for Pascal realization is established at National Physical Laboratory India (NPLI) in 1982 with the collaboration of National Institute of Standards and Technology (NIST), USA. The UIM has the measuring range of 1 Pa–130 kPa with the expanded uncertainty of Q (0.0092 Pa, 7.2×10^{-6} of the reading) at $k = 2$ calculated as per the guidelines are given in ISO guide to the expression of uncertainty. The UIM is a liquid column manometer (LCM) where mercury is used as the liquid medium [1,2] for the time of flight measurement. UIM possesses W-tube structure of three mercury columns, and these tubes are inserted in a reservoir filled with mercury (shown in Fig. 1). Among these three columns, the center column is used as measurement column having 1 m length and 8 cm diameter approximately and remaining side columns are much smaller than the center column lengthwise, used as a pressure test ports. The UIM is based on the principle that the pressure is directly proportional to the height of the liquid column and the pressure measured is given by $\Delta p = h\rho g$, where h is the height of the mercury column, g is the acceleration due to gravity and ρ is the density of the medium (i.e., mercury). 'g' is calculated experimentally at the location of UIM with an accuracy of ppm level and theoretically calculated ρ_{20}, the density of medium at 20 °C is used which further gets corrected according to a temperature of UIM by six platinum resistant thermometers (PRTs) fixed at the various location of the UIM mercury column. The differential length (h) of the column height is calculated by the difference in the height of the central column with the average height of side columns.

The height of the mercury column is calculated in terms of wavelengths [2] using the fringe counting pulsed interferometer [3,4] and the speed of the ultrasonic wave in mercury. The ultrasonic wave of nominal frequency 10 MHz is used because of its uniform speed in homogenous liquid medium and high-resolution sensitivity. The theoretical value of the speed of the ultrasonic wave at 23°C is used in the

* Corresponding author. CSIR-National Physical Laboratory (CSIR-NPL), Dr. K. S. Krishnan Road, Delhi, 110012, India.
E-mail address: ashok553@nplindia.org (A. Kumar).

https://doi.org/10.1016/j.vacuum.2019.04.023
Received 1 February 2019; Received in revised form 11 March 2019; Accepted 12 April 2019
Available online 18 April 2019

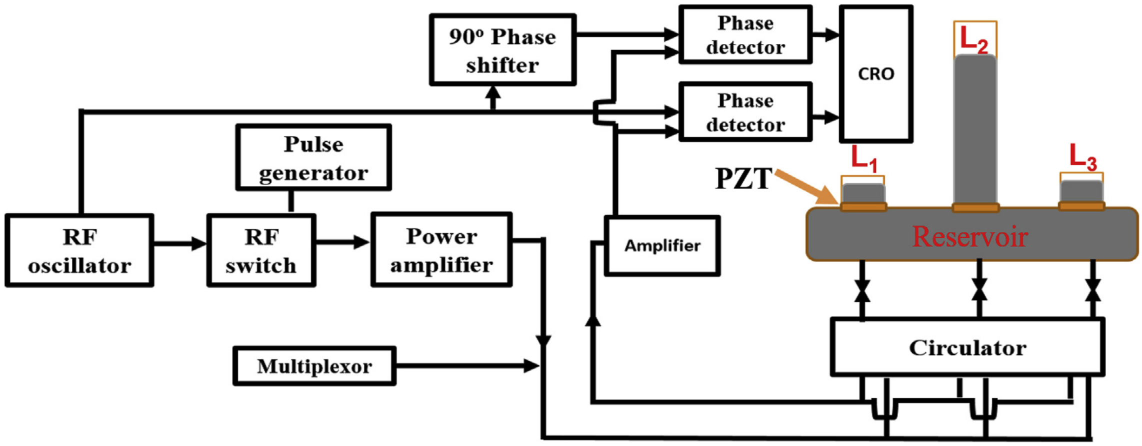

Fig. 1. Block diagram showing the UIM and its connection with various hardware and electronics.

equation which is further corrected according to mercury temperature of the UIM chamber. For the calculation of column length, an ultrasonic wave of a frequency in the range of 9.3–10.6 MHz is generated by RF oscillator as a carrier wave which is used to carry a short pulse of 15μs, using a pulse generator. The lead zirconate titanate $PbZr_xTi_{1-x}O_3$ (PZT) transducers are mounted at the bottom of each mercury column in UIM (shown in Fig. 1) which convert the electrical signal to a mechanical analog of a short ultrasonic wave train which sent vertically upward to the column to measure the column height. These signals move towards the top surface of mercury and then reflect back to the transducer where a part of energy revert to electrical signals and remaining travels back to mercury column, this process continues until all of its energy converts into the electrical signal. Each time an echo is produced in the form of an electrical pulse which is amplified and then further detected by the phase sensitive detectors, and it was found that there is a phase shift of 90^0 between the reference signal and received echo.

The change in the length of the mercury column originates the change in the corresponding phase angle of ultrasound echo and hence resulting quadrature signals $Y_1 = A' \cos(k'L)$ and $Y_2 = A' \sin(k'L)$ where A' is the amplitude of the signals, Y_1 and Y_2 are the vectors from the origin, and λ is wavelength. As path difference of the electric pulse is given by the integral multiple of half of the wavelength (λ) or in other words it can be said that the change in column length is monotonically proportional to the change in the wavelength of the ultrasonic wave and its phase, therefore it can be easily understand that if column length changes with half of the wavelength of an ultrasound wave then the received signal or echo have the rotation of 2π, i.e., a full wave cycle and if the length change by full wavelength then received signal has the rotation of 4π, i.e., two full wave cycles this process continues.

1.1. Theoretical representation of output signals and calculation of pressure

The wave with a carrier angular frequency (ω) travels through the mercury column of length (L) and undergo multiple reflections between the uppermost layer of mercury and the transducer. During this process, the nth order echo is picked up and detected by the phase sensitive detectors with continuous reference signals given by equation (1) in the form of frequency,

$$y_1 = A\cos(\omega t) \text{ and } y_2 = A\sin(\omega t) \quad (1)$$

where A is the amplitude of the reference signal and $\omega = 2\pi f$ where ω is the carrier angular frequency.

The received signals by phase sensitive detectors are represented by equation (2)

$$Y_1 = A\cos(\omega t - 2knL) \text{ and } Y_2 = A\sin(\omega t - 2knL) \quad (2)$$

Using trigonometric relations, equation (2) can be re-written as with absorbing all constants in the amplitude of wave (A')

$$Y_1 = A' [\cos(2knL) + \cos(\omega t - 2knL)] \quad (3a)$$

$$Y_2 = A' [\sin(2knL) + \sin(\omega t - 2knL)] \quad (3b)$$

where k is the wave number given by and $2\pi/\lambda$ and A' is the amplitude of the resultant signals.

The first terms of the wave equations (3a) and (3b) represent sinusoidal functions of column length (L). The second terms are high-frequency signals which are suppressed by low pass filters.

Hence the signals received after passing through low pass filters can be represented by the equation given below:

$$Y_1 = A' \cos(2knL) \quad (4a)$$

$$Y_2 = A' \sin(2knL) \quad (4b)$$

The UIM algorithm used a particular echo of the nth order, i.e., n is a constant. So, we can write $k' = 2kn$ in equations (4a) and (4b). Hence we can rewrite equations (4a) and (4b) as follows:

$$Y_1 = A' \cos(k'L) \quad (5a)$$

$$Y_2 = A' \sin(k'L) \quad (5b)$$

when the $k'L$ changes by 2π, then the received signals of equations (5a) and (5b) go through full wave cycle. So, the change in the length L for a full wave cycle or fringe is given by $\Delta L = \lambda/2n$.

The signals are given by equation (5a) and (5b) have a phase change of 90° with each other, these two signals can be in any of the quadrants. To observe that change, ΔL/quadrant can be written as $\Delta L = \lambda/8n$.

The signals are connected with multiplexor which is used to count the number of fringes with count(s) per quadrant with a change in length of the column in steps of $\Delta L = \lambda/8n$. There may be some fractional fringes which also have been taken care to improve the sensitivity. So, the fractional fringe (f_r) contribution to column length is obtained by equation (6)

$$f_r = (1/2\pi)\tan^{-1}(Y_1/Y_2) \quad (6)$$

The full fringes as well as the fractional fringes are observed and recorded to measure the length very precisely. The column length at a particular pressure for all 44 frequencies in the range of 9.3–10.6 MHz with unevenly spaced frequency is calculated using the window based software along with the associated uncertainty.

The length of the column is related to the number of fringes [5,6], which is given by equation (10). These column lengths are used to calculate the differential length which is the net mercury column height. The pressure is measured inside the UIM by calculating the optical path between the reference level and the uppermost surface of the mercury column. So, that optical path is the differential length (h)

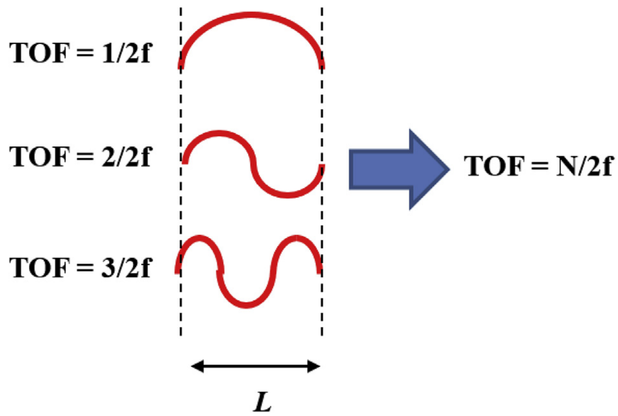

Fig. 2. Explains the relation between *TOF* and frequency of the electrical signal in the cavity formed in mercury column between the transducer and mercury-mercury vapor interface, where *L* is the optical path or length of column and *N* is the positive integer and *f* is the frequency of the electrical signal.

which can be obtained using the formula given below

$$Differential\ length\ (h) = L_2 - \frac{L_1 + L_3}{2} \quad (7)$$

where L_1, L_2, and L_3 are lengths of the mercury column in the side column 1, center column and side column 2, respectively. Time of flight (*TOF*) technique is used to calculate the column length. The time taken by a short electric pulse to travel from transducer to interface of mercury and mercury vapor is known as the time of flight (*TOF*). *TOF* is given by the integral multiple of half of the reciprocal of the frequency of the electrical signal as explained in Fig. 2 i.e. $TOF = N/2f$.

In the case of UIM, *N* is replaced by the number of fringe counts, i.e., $F + f_r$, We can obtain the *TOF* equation as follows;

$$TOF = (F + f_r)/2f \quad (8)$$

Then the length of column (*L*) is given by

$$L = Ss\ X\ TOF \quad (9)$$

Speed of sound (Ss) with temperature correction is given by $S_{23}\{1 - \alpha_s(t_m - 23)\}$ and S_{23} is the speed of sound at 23 °*C* is given by 1449.441 m/s [7].

Using equations (8) and (9), the length of the column (*L*) can be written as follows;

$$L = S_{23}\ (F + f_r)\ (1 - \alpha_s(t_m - 23))/2f \quad (10)$$

F = number of full fringes
f_r = value of fractional fringe
f = frequency of the ultrasonic signal
α_s = temperature coefficient of density of mercury at 20 °*C* = 3.032×10^{-4} °C^{-1}

Using equation (10) the column lengths of all three columns can be calculated using equations given below

$$L_1 = S_{23}\ (F_1 + f_{r1})\ \{1 - \alpha_s(t_m - 23)\}/2f \quad (11a)$$

$$L_2 = S_{23}\ (F_2 + f_{r2})\ \{1 - \alpha_s(t_m - 23)\}/2f \quad (11b)$$

$$L_3 = S_{23}\ (F_3 + f_{r3})\ \{1 - \alpha_s(t_m - 23)\}/2f \quad (11c)$$

where F_1, F_2 and F_3 are full fringe counts and f_{r1}, f_{r2} and f_{r3} are fractional fringe counts of side column 1, center column and side column 2, respectively. As the pressure is measured by UIM is based on the formula given by

$$Differential\ pressure\ (\Delta p) = h\rho g$$

Mercury density (ρ) according to the temperature of UIM chamber is given by

$$\rho = \rho_{20}/\{1 - \alpha_d(t_m - 23)\} \quad (12)$$

where ρ_{20} is density of mercury at 20 °C = 13545.855 kg/m^3 [8] and α_d = temperature coefficient of density of mercury = 181.15×10^{-6} °C^{-1} [9].

Using equations (7) and (12), we get

$$\Delta p = \frac{\rho_{20} g \{L_2 - (L_1 + L_3)/2\}}{1 + \alpha_d(t_m - 20)} \quad (13)$$

g = local acceleration due to gravity = 9.79124184 m/s^2 calculated at the location of UIM with the uncertainty of 2 ppm.
t_m = temperature of UIM chamber in °*C*.

Combining (11) and (13), we get the general equation to calculate the pressure measured by UIM,

$$\Delta p = \frac{\rho_{20} g S_{23} \left\{\frac{(F_2 + f_{r2}) - (F_1 + fr_1 + F_3 + f_{r3})}{2}\right\}\{1 - \alpha_s(t_m - 23)\}}{2f\{1 + \alpha_d(t_m - 20)\}} \quad (14)$$

Hence equation (14) is used to calculate the pressure at a high level of accuracy.

The article highlights various factors of uncertainties contributing to the total uncertainty which further validates the measurements, measurement process and functionalities of phaser shape and magnitude since the application of pressure at test port changes the column length which leads to change in the amplitudes and phase of each received echo. As the performance of UIM has been evaluated time to time through many bilateral comparisons with NIST, USA, BIPM CCM PK-10 [10], and recently with ongoing APMP.MP K4 (2018-19) key comparison [11]. The UIM has been functional at NPLI since last 36 years; however, the present results authenticate the mechanical and electronic stability of the primary pressure standards. These results nearly matched with the results of key comparisons which is extremely helpful as the primary standard for the calibration for many gauges like air piston gauge, force balanced piston gauge and various secondary standards for pressure measurement with the uncertainty varying from part per million of measurement to several percentages of reading at k = 2.

2. Results & discussion

2.1. Current scenario of UIM

In many national metrology institutes, UIMs had been established which were being compared time to time under key comparisons or bilateral comparison. The NPL, India (using the UIM) had participated in BIPM key comparison (CCM PK-10) in 1994 as shown in Fig. 3 [10] which indicates that the maximum difference in the measurement of the effective area of piston-cylinder among participant laboratories was in the range of 10^{-5} *ppm* at the pressure of 31 kPa. However, nowadays most of the leading NMIs (except NIST USA) have been facing problems to maintain and participate in measurement process due to old electronics, hardware, and unavailability of compatible electronics.

The paper deals with a detailed study of the variation of signal properties, i.e., amplitudes, phase angles and oscillations as a function of pressure or mercury length. These parameters have never been studied in detail for NPLI UIM. The pressure measurement has carried out in new technical and environmental conditions. The window based software has replaced the old DOS-based software to calculate the pressure. Apart from software, electronics of the circulator has also modified; the new circulator is fabricated with new microelectronics that provides low noise, less heat dissipation and efficient in signal communication. Some part of UIM hardware/vacuum chamber is also changed to avoid any leakage and provide higher order of background pressure. In this context, old rubber O-ring based sealing is changed

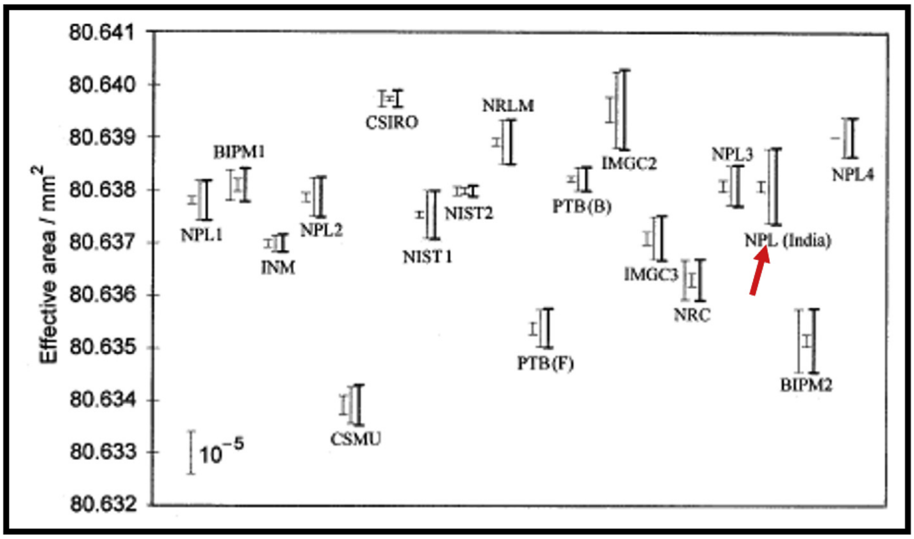

Fig. 3. Effective area values are compared during key comparison at the pressure of 31 kPa in absolute mode and the data of NPL (India) complete with most of the NMIs (reproduce from ref. 10).

with copper gasket based compact flange. Hence it is the need of time for thorough studies on various aspects of uncertainties and phase measurements of UIM. We have taken the observations for column lengths associated with uncertainties and phase measurement for different pressures in the range of 1 Pa–130 kPa for 44 frequencies, explained in detail in next sections.

2.2. Ultrasonic wave properties measurements at various pressures

The variation of some fringes along with amplitudes of signals used in measuring pressure are also studied in detail (shown in Fig. 4) for all 44 frequency data points. These signals are expressed by equations (5a) and (5b) with the phase difference of 90° as it is evident from Fig. 4. Ideally, for a given pressure the amplitudes of these signals should be the same, but experimentally it can be seen that the amplitudes are slightly different which causes the uncertainty in measurement. However the differences in amplitudes are not significant, so the uncertainty contribution due to this difference is very less. At lower pressure, amplitudes are nearly length independent but as pressure increases the amplitudes become dependent on length and as evidence from Figs. 4 and 5. It suggests that amplitude decreases with increase in pressure or differential length or in other words, it can be said that the amplitude of the signal is inversely proportional to the length of the column. As it can be seen also from Fig. 5 that the amplitude from 1 to 1000 Pa varies with same amount in same range and it's variation is not distinguishable because the variation in pressure is length independent in this pressure range whereas 10 kPa onward the amplitude decreases and move on decreasing towards increase in pressure up to 130 kPa since it becomes length dependent. One more physical quantity in Fig. 4 to focus on, i.e., number of fringes or oscillations increases with an increase in column length for the same number of frequency points. The period of two consecutive pulses is of the order of millisecond time scale that means after a fixed interval next pulse is launched till the measurement completes. A short ultrasonic wave train is launched, out of these pulses, one has come out from the transducer, and another is just put on hold which is next to come out. Therefore, if pressure increases, column length increases, the number of oscillations increases. In a reverse mode, it can also be explained by equation (14) that pressure is directly proportional to the number of fringe counts. Therefore, with an increase in pressure, a number of fringe counts increases. The variations in amplitudes and phase angle (shown in Figs. 4 and 5) ultimately provide the uncertainty in pressure measured by the UIM.

2.3. Experimental uncertainty measurement of UIM

Differential lengths are calculated using equation (7) at various pressure points in the range of 1 Pa–130 kPa at 44 frequency points. The first data point in figures 6 to 11 belongs to zero pressure (mercury vapor pressure) point. There are broadly two types of uncertainty which can be calculated using these data; (i) average uncertainty: each pressure point provides 44 data points along with associated uncertainties, these uncertainties are averaged to get the average uncertainty and (ii) standard deviation of mean: it is the standard deviation of mean of 44 data points. We have plotted average uncertainty and standard deviation of mean in length measurement as a function of differential mercury column length in the range of 0.001–1000 mm under corresponding pressure shown in Fig. 6 and Fig. 7, respectively. It can be observed from Fig. 6 that the average uncertainty is more or less constant for individual columns and is independent of length whereas above 10 mm this uncertainty increases with pressure. A significant linear change in uncertainty can be seen in center column because it becomes length dependent above 10 mm and amplitude of signals in center column decreases with increase in pressure. Similarly, Fig. 7 suggests that standard deviation of mean rises significantly in center column with differential length or pressure and that is because of decreasing amplitude of signals in the center column.

The combined uncertainty is calculated to see the combined effect of both types of uncertainties by taking the root sum square of average uncertainty and standard deviation of the mean of each column (shown in Fig. 8). Finally, total uncertainty in differential length is also calculated by taking root sum square of the combined uncertainties of all the three columns as shown in Fig. 9 to obtain one value of uncertainty for each differential length.

As it is evident from Fig. 7 that the uncertainty at lower pressure is independent of pressure whereas at higher pressure uncertainty increases more or less linearly with differential length or pressure so there must be a factor called relative uncertainty. Relative uncertainty is calculated theoretically from the uncertainty budget compared with experimentally obtained values at each pressure point in the range of 1 Pa–130 kPa, can be seen in Fig. 10. At lower pressure, i.e., up to 1 kPa, experimental relative uncertainty values decreases linearly with pressure and are more than the theoretical values due to many factors but most importantly temperature and vibrational effect. Whereas at higher pressure it becomes more or less constant and experimental relative uncertainty is less than that of theoretical values (shown in the inset of Fig. 10) because at the high-pressure contribution of vibrational and

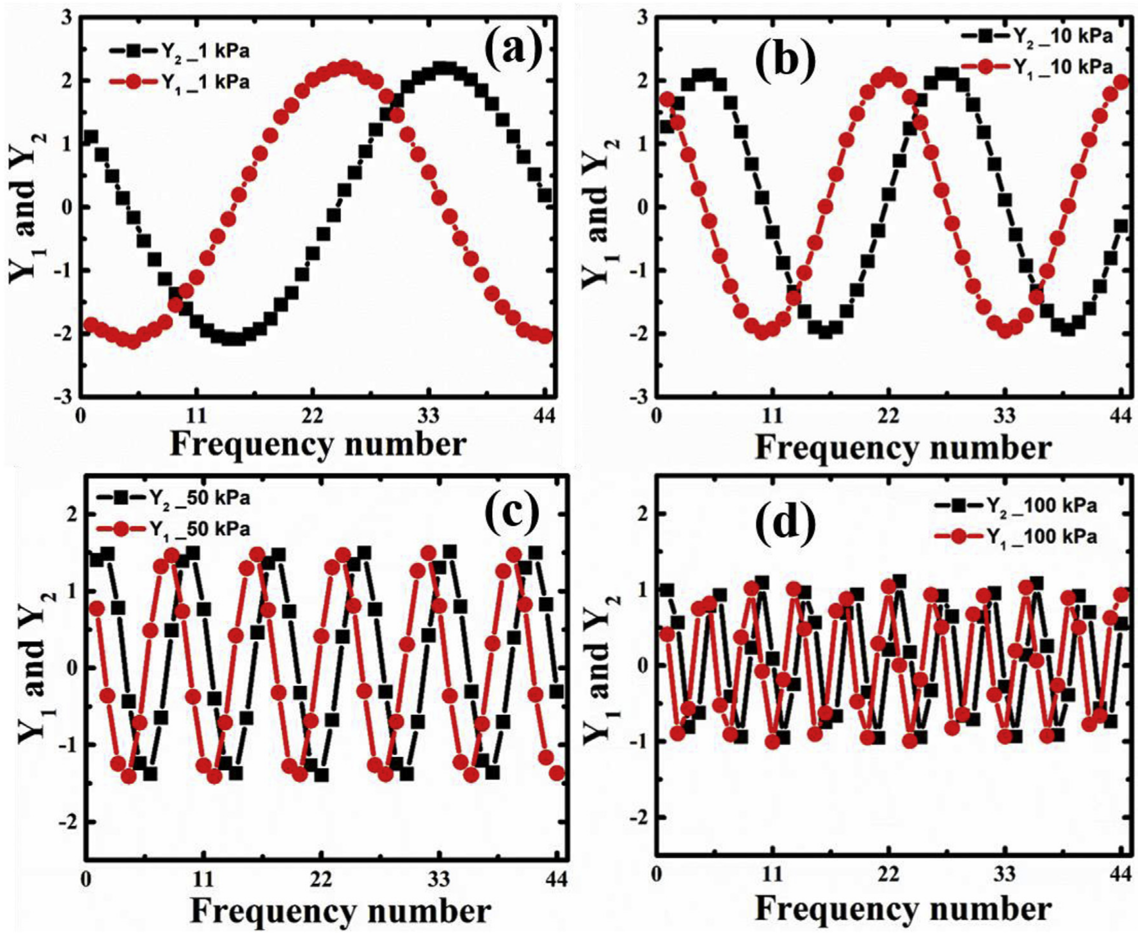

Fig. 4. Describes the electrical signals $Y_1 = A' \cos(k'L)$ (red curve) and $Y_2 = A' \sin(k'L)$ (black curve) formed inside the mercury column with varying pressure: (a) 1 kPa, (b) 10 kPa, (c) 50 kPa and 100 kPa.

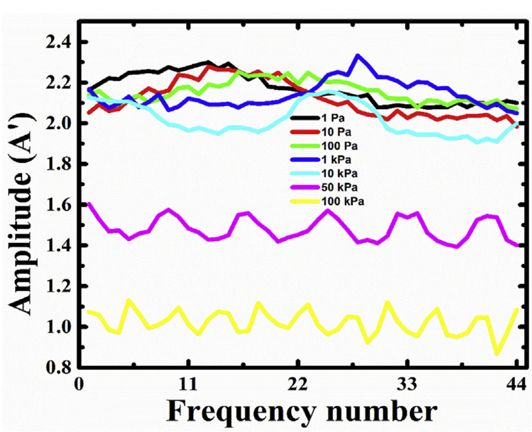

Fig. 5. Describes the amplitudes (A') of electrical signals formed inside the mercury column with varying pressure from 1 Pa to 100 kPa.

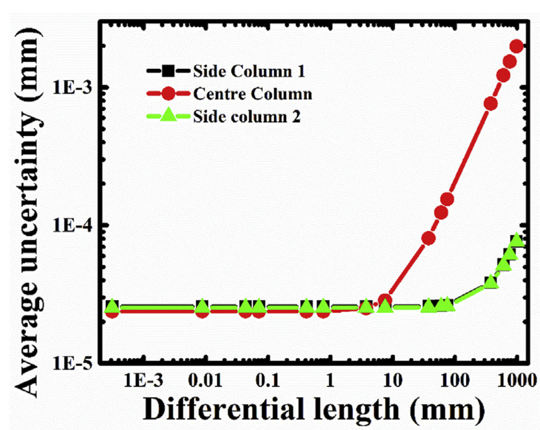

Fig. 6. Average uncertainty of the uncertainties associated with all 44 data points for the three columns at each pressure point in the range are shown with varying differential length in the range of 0.001–1000 mm.

temperature effects in uncertainty are not significant. In conclusion evaluation of relative uncertainty, the experimental and theoretical expanded relative uncertainty at $k = 2$ were obtained as 5.6×10^{-6} and 7.2×10^{-6} respectively at higher pressure. The relative uncertainty is combined with associated pressure and the resolution part; it gives the total uncertainty at each pressure point. Fig. 11 shows the experimental, as well as total theoretical uncertainty with varying pressure, these two curves, are in total agreement with each other. These values describe that uncertainty is the nearly constant at low pressure because of length independency that's why it is also called as resolution whereas above that pressure it goes linearly with pressure relative uncertainty part starts dominating over resolution part. These uncertainties shown in Figs. 6–11 are matching with the previously measured data [12].

2.4. Uncertainty budget in the pressure measured by UIM

Uncertainty budget for 130 kPa is shown in Table 1 which show the factors contributing to uncertainty calculation with their associated

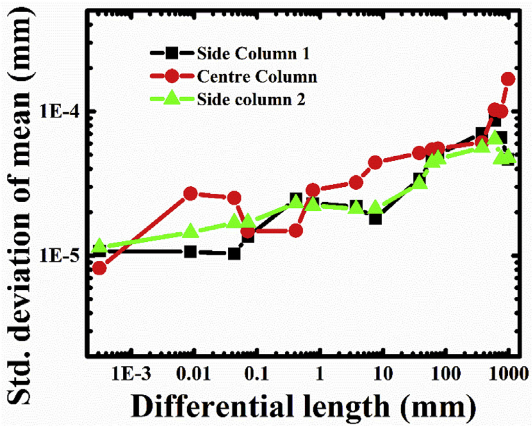

Fig. 7. Standard deviation of mean value of the length of 44 data points for the three columns as a function of differential length measured by UIM.

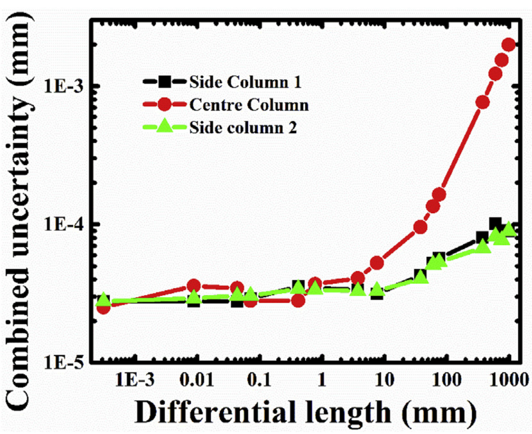

Fig. 8. Combined effect of average uncertainty and standard deviation of mean is shown in the form of combined uncertainty with the varying differential length of individual columns.

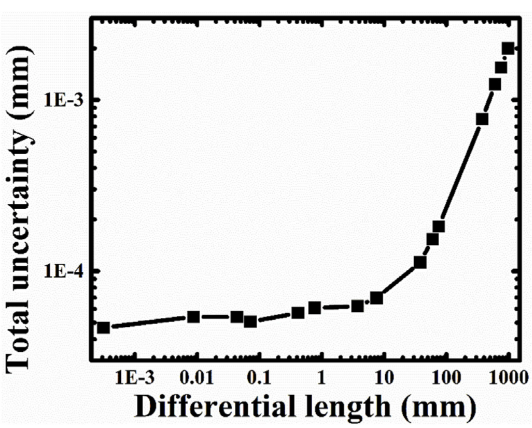

Fig. 9. Total uncertainty is calculated by taking root sum square of the combined uncertainty of all three columns with varying differential length at each pressure point.

pressure dependent and independent uncertainties. The independent part gives the resolution of measuring (UIM) instrument whereas the dependent parts give the uncertainty in pressure measurement. In Table 1, the expanded uncertainty is obtained as per theoretical equation, i.e. $((0.0092\,\text{Pa})^2 + (7.2 \times 10^{-6}.\ p)^2)^{0.5}$ Pa, where p is the measured pressure in Pa. Hence the theoretical expanded uncertainty for the 130 kPa is equal to $= ((0.0092\,\text{Pa})^2 + (7.2 \times 10^{-6}.$

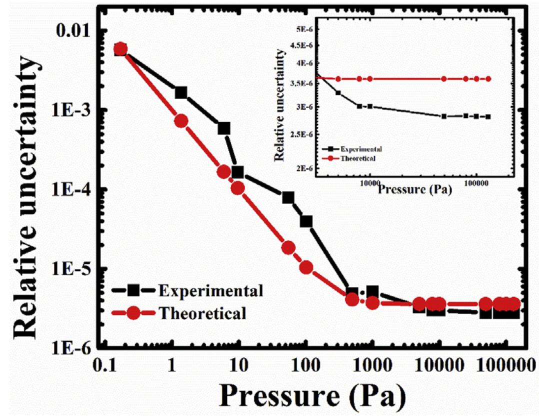

Fig. 10. Variation of theoretical as well as experimental relative uncertainty in pressure is shown with varying pressure.

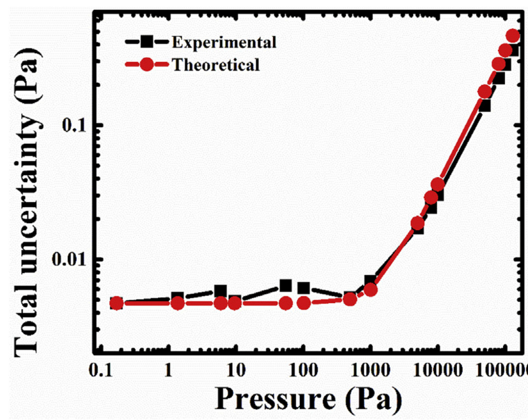

Fig. 11. Experimental and theoretical total uncertainties in pressure measurement of UIM calculated and compared in the pressure range of 1 Pa–130 kPa.

$13 \times 10^4)^2)^{0.5}$ Pa = 0.9320 Pa which is higher than the experimental expanded uncertainty $((0.0092\,\text{Pa})^2 + (5.6 \times 10^{-6} * 13 \times 10^4)^2)^{0.5}$ Pa = 0.7249 Pa. These values validate the long time stability, reproducibility, accurateness, and uncertainty measurement of UIM from 1 Pa to 130 kPa pressure range.

3. Summary

The UIM is further revalidated over the pressure range of 1 Pa–130 kPa that provides uncertainty in the measurement well within our calibration measurement and capability. The expanded uncertainties in the above-mentioned measurement range matched well with the theoretical value, however, at the low-pressure range the expanded uncertainty sometimes show slightly higher than resolution components that may be due to environmental conditions, but it always gave lower uncertainty in the pressure-dependent measurement range. The signal ultrasonic probe wave amplitude and phase variation and its associated uncertainties as a function of the change in column length are probed which provides satisfactory experimental standard deviation of the mean. The theoretical and experimental evidence confirms the accurateness and long term durability and firmness of pressure measurement uncertainties which further proves that it is still India's apex level primary standard with the lowest uncertainty since last 36 years.

Acknowledgment

The authors would like to thank Dr. D. Arun VijayKumar (Retired Scientist, CSIR-NPL) for suggestions and motivation time to time. The

Table 1
Uncertainty budget of Pressure measurement of UIM at 130 kPa.

Quantity	Estimate	Uncertainty	Probability distribution	Type	Degrees of Freedom	Uncertainty Contribution $(U_i(y))^2$	
(X_i)	(x_i)	Ux_i				Independent	Dependent
Density of Hg - ρ_{20} (kg/m^3)	13545.855	0.012	Normal	B	Infinity		1.41E-02
Accln. Due to Gravity g (m/s^2)	9.791242	1.96E-06	Normal	B	Infinity		6.76E-04
Speed of Sound in Hg S_{23} (m/s)	1449.441	0.0021	Normal	B	Infinity		3.65E-02
Temperature - t (oC)	22.0	0.005	Normal	B	Infinity		9.91E-02
Thermal coeff.of Density of Hg α_D (oC^{-1})	1.81E-04	5.00E-08	Normal	B	Infinity		1.69E-04
Thermal coeff.of Speed of Sound in Hg - α_S (oC^{-1})	3.03E-04	7.00E-08	Normal	B	Infinity		8.28E-05
Fringe Counting - Fr (Pa)		0.001	Normal	A	127	1.00E-06	
Ultrasonic Frequency - f (Hz)	1.000E + 07	3.00E-01	Normal	B	Infinity		1.52E-05
Ultrasonic Phase (Pa)		0.260	Normal	B	Infinity		6.76E-02
Verticality (Pa)		7.80E-03	Normal	B	Infinity		6.08E-05
Tilt (Pa)		3.00E-04	Normal	A	20	4.00E-08	
Zero instability (Pa)		0.0043	Normal	A	31	1.85E-05	
Static Head Correction δph (Pa)		1.43E-02	Normal	B	Infinity		2.04E-04
Ref Pressure - pref (Pa)	0.22	0.001	Normal	B	Infinity	1.44E-06	1.00E-06
				Uncertainty (m^2)		4.6E-3	4.67E-01
						Abs. value	Rel. value
			Relative uncertainty (at k = 1)			0.0046	3.6E-06
			Expanded relative uncertainty (at k = 2)			0.0092	7.2E-06

authors also want to thank Dr. D. K. Aswal (Director, CSIR-NPL) and Dr. Ranjana Mehrotra (Head, Physico-Mechanical Metrology Division, CSIR-NPL) for their constant encouragement. Authors also want to thank CSIR-NPL for the partial funding to accomplish the project. Vikas Narayan Thakur wants to thank AcSIR, CSIR-NPL for pursuing Ph.D. program and UGC for fellowship to pursue the Ph.D. program.

Appendix A. Supplementary data

Supplementary data to this article can be found online at https://doi.org/10.1016/j.vacuum.2019.04.023.

References

[1] C.R. Tilford, New developments in barometric range pressure standards, Natl. Conf. Stand. Lab. Workshop and Symp. 1988 35-41 to 35-15 https://www.nist.gov/sites/default/files/documents/calibrations/ncsl88.pdf.
[2] P.L.M. Heydemann, C.R. Tilford, R.W. Hyland, Ultrasonic manometers for low and medium vacua under development at the National Bureau of Standards, J. Vac. Sci. Technol. 14 (1977) 597–605, https://doi.org/10.1116/1.569158.
[3] P.L.M. Heydemann, A fringe-counting pulsed ultrasonic interferometer, Rev. Sci. Instrum. 42 (1971) 983–986, https://doi.org/10.1063/1.1685319.
[4] C.R. Tilford, A fringe counting laser interferometer manometer, Rev. Sci. Instrum. 44 (1973) 180–182, https://doi.org/10.1063/1.1686077.
[5] C.R. Tilford, Analytical procedure for determining lengths from fractional fringes, Appl. Opt. 16 (1977) 1857–1860 http://www.ncbi.nlm.nih.gov/pubmed/20168822.
[6] P.L.M. Heydemann, Determination and correction of quadrature fringe measurement errors in interferometers, Appl. Opt. 20 (1981) 3382, https://doi.org/10.1364/AO.20.003382.
[7] C.R. Tilford, The speed of sound in a mercury ultrasonic interferometer manometer, Metrologia 24 (1987) 121–131, https://doi.org/10.1088/0026-1394/24/3/003.
[8] A.H. Cook, Precise measurements of the density of mercury at 20 degrees C II. Content method, Philos. Trans. R. Soc. A Math. Phys. Eng. Sci. 254 (1961) 125–154, https://doi.org/10.1098/rsta.1961.0013.
[9] K.-D. Sommer, J. Poziemski, Density, thermal expansion and compressibility of mercury, Metrologia 30 (1994) 665–668, https://doi.org/10.1088/0026-1394/30/6/023.
[10] M. Perkin, R. K hler, P. Riety, T. Skrovanek, E.C. Morris, C.R. Tilford, C.D. Ehrlich, A. Ooiwa, G. Eichorn, J. J ger, G.F. Molinar, A.H. Bass, A.C. Gupta, Comparison of pressure standards in the range 10 kPa to 140 kPa, Metrologia 35 (1998) 161–173, https://doi.org/10.1088/0026-1394/35/3/4.
[11] The BIPM Key Comparison Database: https://kcdb.bipm.org/AppendixB/KCDB_ApB_info.asp?cmp_idy = 135&cmp_cod = APMP.M.P-K4&page = .
[12] D.R. Sharma, D.A. Vijayakumar, Measurement uncertainty estimation in real experimental conditions of ultrasonic interferometer manometer established at NPL, India, Vacuum 81 (2007) 1051–1061, https://doi.org/10.1016/j.vacuum.2006.12.015.